Stress Gradient at the α_S/β Interface in a Ti-6Al-4V Alloy

Philippe Castany, Florence Pettinari-Sturmel, Joël Douin, Armand Coujou

Centre d'Elaboration de Matériaux et d'Etudes Structurales, BP 94347, 31055 Toulouse Cedex 4, France

TEM in situ tensile tests have been performed on a duplex Ti-6Al-4V alloy at room temperature. A stress gradient at the interfaces between α_S and β plates in lamellar colonies has been measured from the curvature radius evolution of moving dislocations emitted from these interfaces. Two different methods are used and compared for the measurements. The stress increases from 85 MPa at the centre of the α_S plate to 225 MPa at 100 nm from the interface. The average stress in α phase in lamellar colonies is about 155 MPa. The origin and effects of this stress variation are discussed. It appears that this variation results from the stress field induced by dislocations present at α_S/β interfaces before deformation. The stress values are then compared with previous macroscopic results.

Keywords: *Ti-6Al-4V, transmission electron microscopy (TEM), in situ, tensile test, dislocations, stress*

1. Introduction

Titanium alloys are widely used in aeronautic applications because of their good specific mechanical properties. The most used of them is the Ti-6Al-4V alloy which is a two-phase alloy with a h.c.p. α phase and a b.c.c. β phase. Its microstructure depends on the thermomechanical treatments. The duplex microstructure of the investigated alloy consists in primary nodules (α_P) and lamellar colonies (α_S/β) (figure 1a). Our observations indicate that the nodule volume fraction is close to the lamellar colony one in agreement with recent results by Bridier et al. [1]. The details of a lamellar colony are illustrated in figure 1b: generally α_S plates are regularly separated by thin β plates except where the β phase is discontinuous (e.g. A and B in figure 1b). The total volume fraction of the β phase has been estimated around 3%. In lamellar colonies, the two phases have a near-Burgers orientation relationship close to:

$$(1\,0\,1)_\beta \,//\, (0\,0\,0\,1)_\alpha \text{ and } [1\,\bar{1}\,\bar{1}]_\beta \,//\, [2\,\bar{1}\,\bar{1}\,0]_\alpha \qquad (1)$$

The presence of this phase noticeably influences the mechanical properties.

The elementary deformation micromechanisms of Ti-6Al-4V alloys are not well known. They have been earlier studied in cryogenic conditions using in situ transmission electron microscopy (TEM) deformation technique [2] or from post mortem observations in other similar titanium alloys: at room temperature, the role of the interfaces in lamellar structures has been studied for prismatic [3] or basal glide [4] as the strengthening due to the presence of short range order in nodular alloys [5]. Our aim is then to contribute to the understanding of elementary deformation micromechanisms which are the cause of the Ti-6Al-4V strengthening: the role of interfaces [6], the effects of the core structure of dislocations [7] and the contribution of short range order [8] are then studied using in situ TEM deformation experiments. This technique is the only one allowing the study of dislocation dynamic under stress and temperature.

We have shown previously that dislocations are always first emitted from α/β interfaces in this alloy in lamellar colonies as well in nodules [6,7]. TEM in situ deformation experiments will be used in the present paper to evaluate the stress variation if any, in α_S plates in the close vicinity of the α_S/β interfaces in lamellar colonies; this variation can be also an explanation for such emission of dislocations. The stresses have been measured from the dislocation shapes when dislocations are stopped in pseudo-equilibrium positions during their motion.

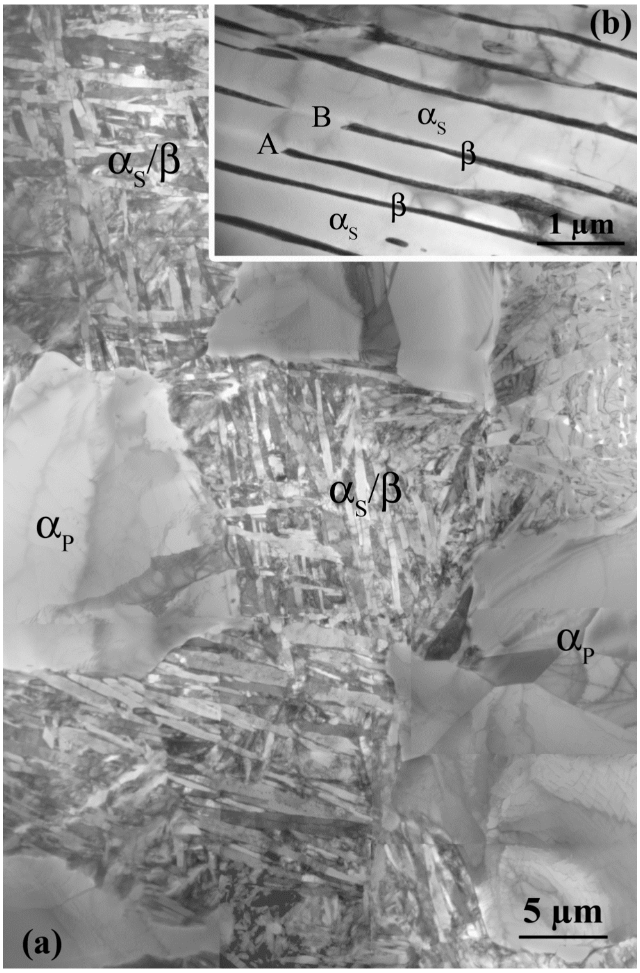

Figure 1. Microstructure of the investigated alloy with primary alpha nodules α_P and lamellar colonies α_S/β (a) and a detailed view of a lamellar colony with α_S and β plates (b).

The presented results on the deformation micromechanisms of a Ti-6Al-4V alloy are a previous work to the study of the influence of the surface treatments on this alloy deformation.

2. Experimental results

In situ tensile tests have been performed at room temperature with a Gatan straining holder. TEM observations were made with a JEOL 2010 equipped with a SIS CCD camera. Details of the TEM in situ deformation technique are given in previous studies [9].

The figure 2 shows the emission of a dislocation loop from an α_S/β interface in a α_S plate. This loop is arrowed *d* on figure 2a and expands on the next images.

Dislocations in this lamellar colony glide in the basal plane and have a Burgers vector $\mathbf{b} = a/3\left[11\bar{2}0\right]$ determined by the **g.b**=0 invisibility criterion. This Burgers vector is an **a**-type vector as the large majority of dislocations in titanium alloys deformed at room temperature [1,3-5,7].

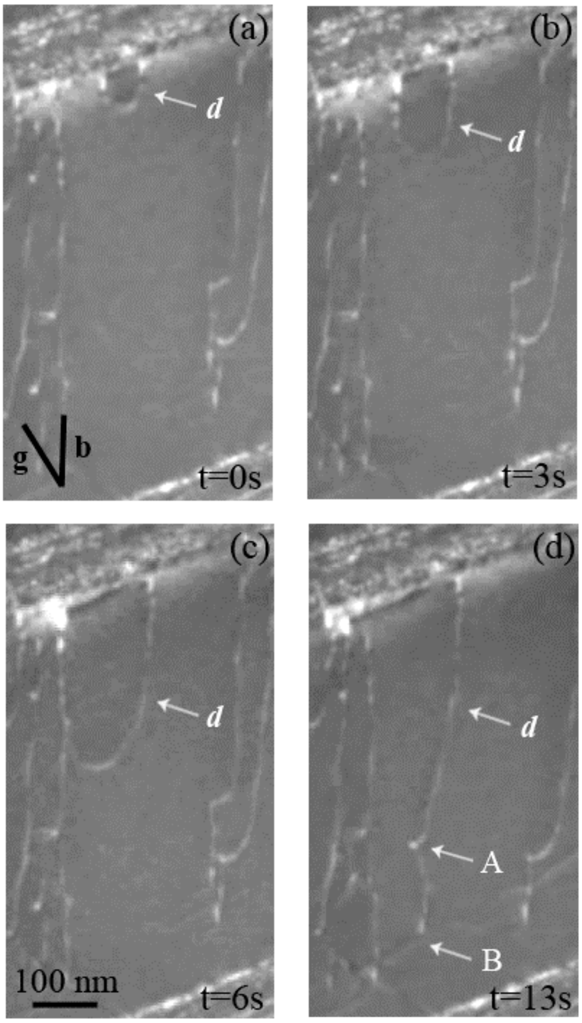

Figure 2. Emission and expansion of a dislocation loop in a α_S plate from an α_S/β interface during a TEM in situ experiment.

We can remark that the dislocation takes a preferential orientation along this screw direction and only the near-edge segment is bowed. Departure from the screw orientation can be favoured by the existence of pinning points as in A figure 2d. Finally the dislocation loop emerges on the sample surface at the point B and the slip plane trace is thus visible.

As measured from such experiments exemplified in figure 2, the edge segment velocity is about 100 times larger than the screw segment one. Moreover, the screw segments glide by a well known "locking-unlocking mechanism" [10] and remain essentially rectilinear due probably to their three-dimensional core structure spread in different cozonal planes as in α-titanium [10-12]. The movement of screw dislocations is then jerky. Cross-slip is frequent and the open loop mechanism is the main mechanism for dislocation multiplication. Many intrinsic pinning points are present on screw segments and extrinsic ones are less frequent.

The stress measurements have been performed when dislocations are temporarily stopped in pseudo-equilibrium positions. We have used two different methods:

- The first one is the classical method using the local curvature of edge or mixed dislocation segments which are flexible and so in equilibrium with the applied stress contrary to the screw segments which are here rectilinear because of their core structure. This method is performed under the framework of isotropic elasticity. Schematically, assuming a constant friction stress, the curvature radius *R* of a dislocation segment pinned on two fixed points is inversely proportional to the force τb acting on it, that is $R = T/\tau b$, where *T* is the line tension of the dislocation, τ the local stress value and *b* this Burgers vector modulus. *T* is depending on the character θ of the dislocation [13]:

$$T = \frac{\mu b^2}{4\pi} \frac{1 + \upsilon - 3\upsilon \sin^2 \theta}{1 - \upsilon} \ln \frac{R_0}{b} \qquad (2)$$

where μ is the shear modulus, ν the Poisson's ratio and R_0 the outer cut-off radius. The relation $R = T/\tau b$ is then only valid locally, assuming that *T* does not vary much with θ. The figure 3b is an illustration of this method. The dislocation is here bowed between its two screw segments. The measured curvature radius is projected onto the image plane and it is then necessary to correct it.

- The previous method is not enough precise to correctly measure a stress variation, and to obtain a better precision on the stress measurement, the complete dislocation loop equilibrium shape under stress has been calculated in its slip plane with non-constant line tension *T*. We have performed our calculations under the framework of anisotropic elasticity using the software DISDI [14,15]. We have used the elastic constants of α-titanium [16]. The local stress is then determined by finding the value of τ which makes the calculated shape coincide with the dislocation image. An example is shown on figure 3c where the calculated shape is superimposed on the micrography and fits the dislocation line. The screw segments being rectilinear because of their core structure, it is not possible to superimpose the calculated shape on all the screw segment length. The screw segments act as pinning points and the calculated shape is then superimposed only between these two segments (dashed line in figure 3c). Notice that the slip plane projection onto the figure plane is also taken into account in the calculation.

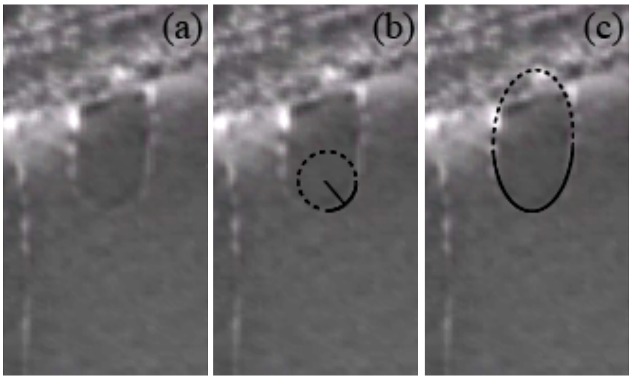

Figure 3. Local stress measurement method on a dislocation loop (a). For the first method, a circle is superimposed on the dislocation and the curvature radius is then measured (b). The second method consists with the superposition of a calculated dislocation shape on the dislocation line (c).

These two methods have been used to determine the stress for different dislocation positions in relation to the α_S/β interface. The results are plotted in figure 4. The stress is not constant: it decreases from 225 MPa to 85 MPa respectively from a distance at 100 nm from the interface to the α_S plate centre. It was not possible to measure the stress closer to the interface because of the tilt of the sample. The local stress far from interfaces on pinned dislocations has been also measured about 155 MPa with a standard deviation of 17 MPa.

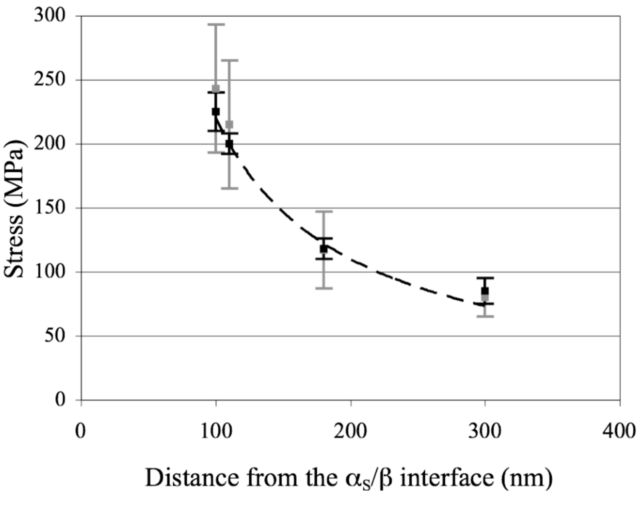

Figure 4. Measured stress as a function of the distance from α_S/β interface. The results using the curvature radius measurement method are in grey and the ones using the calculated shape method in black. The dotted line is a plotted curve function of the inverse distance.

3. Discussion

In situ TEM deformation experiments have allowed to determine and analyse the deformation micromechanisms in a Ti-6Al-4V alloy. The present paper focuses on the estimation of the stress gradient present in α_S plates in the neighbourhood of the α_S/β interface in lamellar colonies. This stress variation has been confirmed by convergent beam electron diffraction (CBED) measurement [17].

The measurement uncertainties are reported on figure 4 for the two methods. These two methods are based on the superposition of a shape (a circle for the curvature radius measurement or the calculated shape) onto the real dislocation line. But the shapes corresponding to several stress values correctly fit the dislocation line because of the thickness of the dislocation line on the micrography and the dislocation configuration. The measurement uncertainty is then estimated by the determination of this range of values which fit well. The measurement method using DISDI is more precise than the one using the curvature radius because the calculated shape fits with a longer dislocation line part. The relative uncertainties are respectively about 7% and 20%.

The results from the two methods being similar, that means crystalline anisotropy has a very weak influence on the stress results. The line tension approximation is then a good approximation for the stress measurement and the shape calculated with the DISDI software gives more precise values.

The measured stresses are the shear stress necessary to the existence of the micromechanisms observed: emission of dislocations from α/β interfaces, movement by locking-unlocking of the screw segments, cross-slip, multiplication. We have measured an higher stress close to the α_S/β interfaces where emission of dislocations occurs. This additional stress can have two origins:

- The stress field due to the elastic compatibility stress between the two phases α and β.
- The stress field created by the dislocations present at the interface between the two phases α and β before deformation.

Greene et al. have shown from finite element method that the compatibility stress in lamellar structures of titanium alloys is probably homogeneous in the plate thickness [18] because of the low volume fraction of the minor phase (here the β phase). A curve function of the inverse distance has been plotted on figure 4 (dotted line). The stress appears inverse proportional to the distance which agrees with the stress field due to dislocations. Moreover, two phases with the Burgers orientation relationship have at the interface **c**-type and **a**-type dislocations in the h.c.p. phase in order to minimize the interface energy [19]. These interfaces between the two plates α_S and β are tilted on figure 2 and seem filled with a lot of dislocations even before deformation. It confirms then that the additional stress close to the α_S/β interfaces is due to these dislocations. Note that elastic compatibility stress has nevertheless an important effect: it slightly favours basal glide in lamellar colonies in comparison with prismatic glide [7,20].

The local stress values measured here have been compared to literature results previously published from macroscopic tests. There is little results performed with conditions that allow a comparison with our results because to compare the macroscopic yield strength at 0.2% with the local stress allowing the mobility of dislocations is not very pertinent in alloys with such complex microstructure. It can be significant only in singlecrystals.

In α_S plates, we have measured an average local stress of 155 MPa. We have shown that the stress increases near the α_S/β interfaces and its value is probably much higher in the very close vicinity of these interfaces. In a Ti-6242 alloy compound of a single lamellar colony, Savage et al. [21] have measured the Critical Resolved Shear Stress (CRSS) for the basal glide which is between 215 and 285 MPa. This values are in the same order of magnitude than our results.

Other studies calculate the CRSS from the yield strength at 0.2% and give values with about 100 MPa higher than the previous ones [1,4]. This difference confronts us with the problem of the comparison of measurements performed at two very different scales. But this difference is understandable: to deform macroscopically a sample at 0.2%, most of the grains must be deformed even the less favourably oriented which need an higher applied stress. But with TEM in situ experiments, only the more favourably oriented grains are deformed. Therefore we obtain the microscopic yield strength in lamellar colonies which is about 155 MPa. Moreover in complex microstructure alloys with several strengthening contributions, it is interesting to determine the microscopic yield strength for each contribution.

As basal and prismatic glides which are the two preferential deformation modes of titanium alloys at room temperature have similar CRSS [1,21] and have similar deformation micromechanisms [7] in Ti-6Al-4V alloys, present results for the basal glide can be generalised for the prismatic glide too.

4. Conclusions

A stress gradient at the α_S/β interfaces in lamellar colonies of a Ti-6Al-4V alloy has been determined from the curvature radius evolution of dislocations during TEM in situ tensile tests. The local stress in the α_S plates increases in the close vicinity of these interfaces. This variation results from the stress field induced by dislocations present at these interfaces before deformation and not from the elastic compatibility stress between the two phases which is constant in the α_S plate thickness.

It is also worth pointing out that:

- From a fundamental point of view, the knowledge of deformation micromechanisms is crucial and, numerous titanium alloys having similar α phase composition and similar microstructure, all these results can most likely be generalised to them.
- The identification of the deformation micromechanisms and the associated microscopic yield strength are essential for modelling: from them, it could be possible to model the bulk alloy and predict macroscopic yield strength from microscopic data like the present measurements and the alloy microstructure.

REFERENCES

1) F. Bridier, P. Villechaise and J. Mendez: Acta Mater. **53** (2005) pp.555-567.
2) A. Ambard, L. Guétaz, F. Louchet and D. Guichard: Mater. Sci. Eng. A **319-321** (2001) pp.404-408.
3) S. Suri, G.B. Viswanathan, T. Neeraj, D.H. Hou and M.J. Mills: Acta Mater. **47** (1999) pp.1019-1034.
4) M.F. Savage, J. Tatalovich and M.J. Mills: Philos. Mag. **84** (2004) pp.1127-1154.
5) T. Neeraj, D.-H. Hou, G.S. Daehn and M.J. Mills: Acta Mater. **48** (2000) pp.1225-1238.
6) P. Castany, F. Pettinari-Sturmel, J. Douin and A. Coujou: Mater. Sci. Eng. A (2007) in press.
7) P. Castany, F. Pettinari-Sturmel, J. Douin and A. Coujou: Acta Mater. submitted.
8) P. Castany, F. Pettinari-Sturmel, J. Douin and A. Coujou: to be published.
9) A. Couret, J. Crestou, S. Farenc, G. Molénat, N. Clément, A. Coujou and D. Caillard: Microsc. Microanal. Microstruct. **4** (1993) pp.153-170.
10) S. Farenc, D. Caillard and A. Couret: Acta Metall. Mater. **41** (1993) pp.2701-2709.
11) S. Naka, A. Lasalmonie, P. Costa and L.P. Kubin: Philos. Mag. A **57** (1988) pp.717-740.
12) D.J. Bacon and V. Vitek: Metall. Mater. Trans. A **33** (2002) pp.721-733.
13) D. Raynor and J.M. Silcock: Met. Sci. J. **4** (1970) pp.121-130.
14) J. Douin, P. Veyssière and P. Beauchamp: Philos. Mag. A **54** (1986) pp.375-393.
15) J. Douin, http://www.cemes.fr/Personnel/douin/Disdi-Page.html
16) E.S. Fisher and C.J. Renken: Phys. Rev. **135** (1964) pp.A482.
17) F. Houdellier and P. Castany: to be published
18) C.A. Greene and S. Ankem: Mater. Sci. Eng. A **202** (1995) pp.103-111.
19) M.R. Plichta and H.I. Aaronson: Acta Metall. **28** (1980) pp.1041-1057.
20) S. Ankem and H. Margolin: Metall. Trans. **11A** (1980) pp.963-972.
21) M.F. Savage, J. Tatalovich, M. Zupan, K.J. Hemker and M.J. Mills: Mater. Sci. Eng. A **319-321** (2001) pp.398-403.